Provided for non-commercial research and education use.
Not for reproduction, distribution or commercial use.

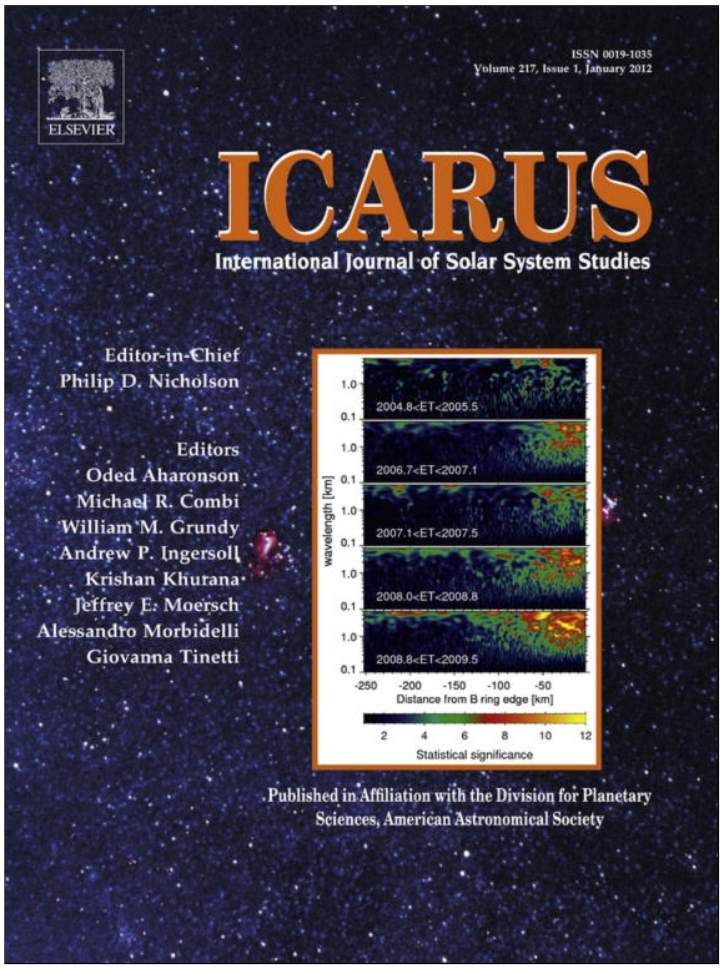


(This is a sample cover image for this issue. The actual cover is not yet available at this time.)

This article appeared in a journal published by Elsevier. The attached copy is furnished to the author for internal non-commercial research and education use, including for instruction at the authors institution and sharing with colleagues.

Other uses, including reproduction and distribution, or selling or licensing copies, or posting to personal, institutional or third party websites are prohibited.

In most cases authors are permitted to post their version of the article (e.g. in Word or Tex form) to their personal website or institutional repository. Authors requiring further information regarding Elsevier's archiving and manuscript policies are encouraged to visit:

http://www.elsevier.com/copyright

Author's personal copy

Icarus 219 (2012) 150–160

Contents lists available at SciVerse ScienceDirect

Icarus

journal homepage: www.elsevier.com/locate/icarus

# Öpik-type collision probability for high-inclination orbits

David Vokrouhlický [a,*], Petr Pokorný [a], David Nesvorný [b]

[a] Institute of Astronomy, Charles University, V Holešovičkách 2, CZ-18000 Prague 8, Czech Republic
[b] Southwest Research Institute, 1050 Walnut St., Suite 300, Boulder, CO 80302, USA

ARTICLE INFO

*Article history:*
Received 20 December 2011
Revised 14 February 2012
Accepted 20 February 2012
Available online 3 March 2012

*Keywords:*
Celestial mechanics
Impact processes
Asteroids
Interplanetary dust

ABSTRACT

The classical Öpik theory provides an estimate of the collision probability between two bodies on bound, heliocentric or planetocentric orbits under restrictive assumptions of: (i) constant eccentricity and inclination, and (ii) uniform circulation of the longitude of node and argument of pericenter. These assumptions are violated whenever either of the orbits has a large inclination with respect to the local Laplace plane or large eccentricity, and their motion is perturbed by an exterior (tidal) gravitational field of a planet or the Sun. In this situation, known as the Lidov–Kozai regime, the eccentricity and inclination values exhibit large and correlated oscillations. At the same time, the longitude of node and the argument of pericenter may have strongly nonlinear time evolution, with the latter being even bound to a small interval of values. Here we develop a new Öpik-type collision probability theory which is valid even for highly inclined and/or eccentric orbits of the projectile. We assume that the orbit of the target is circular and in the local Laplace plane. Such a generalized setting is necessary, as an example, to correctly estimate the terrestrial impact fluxes of sporadic micrometeoroids on high-inclination orbits (notably those from the toroidal source and the associated helion and anti-helion arcs).

© 2012 Elsevier Inc. All rights reserved.

## 1. Introduction

Many problems in planetary science require to determine the collision probability of two bodies residing on the Keplerian orbits with the same focal point. Here we consider the important case in which the collision probability needs to be evaluated in a statistical sense for a large population of bodies. In this case, it is often useful if the probability is averaged over the secular orbital timescale.

The standard theory, used and extended by many researchers, was developed by Öpik (1951) (see also Öpik, 1976; Wetherill, 1967; Greenberg, 1982). In his original formulation, Öpik assumed that the target on a circular orbit is bombarded by a population of bodies on orbits with fixed eccentricity and inclination values.

Öpik's theory was generalized to the case of an eccentric orbit of the target by Wetherill (1967) and Greenberg (1982). A different generalized method was developed by Kessler and Cour-Palais (1978) (see also Kessler, 1981). This more geometrical approach based on the evaluation of the probability density distribution has found a number of applications in planetary science (e.g., Steel and Baggaley, 1985; Steel and Elford, 1986; Sykes, 1990).

In these standard collisional theories, the orbital eccentricity $e$ and inclination $i$ is assumed to be constant during the secular evolution cycle. This is appropriate for small $e$ and $i$ values, where $e$ and $i$ are roughly time-invariant. However, some problems in planetary science require a method that is valid for high eccentricities and/or high inclinations, where the effects of the Lidov–Kozai resonance can be important (e.g., Lidov, 1961, 1962; Kozai, 1962; Morbidelli, 2002).

For example, the dust particles released from long-period comets can be an important component of the zodiacal cloud. If so, it would be important to calculate their impact rates on the Earth (and relate the results to meteor observations), Earth-bound detectors and spacecrafts. Other applications can be found in studies of planetary impact rates in the early Solar System when small bodies were stochastically driven to high-$e$ and -$i$ orbits. In these examples, the secular evolution of orbits clearly violates the assumption of the standard Öpik theory, because $e$ and $i$ are affected by the Lidov–Kozai cycles.

Here we generalize the Öpik theory to account for the Lidov–Kozai cycles of high-$i$ and -$e$ orbits. After mathematical preliminaries in Section 2, we generalize the collisional probability theory in Section 3. In Section 3.3, we test the generalized theory by comparing it with direct $N$-body integrations of orbits. Conclusions are given in Section 4.

## 2. Mathematical preliminaries

We start by introducing mathematical concepts and notation that will be used throughout the paper. Assume a particle on an elliptic heliocentric orbit described using an osculating set of

* Corresponding author.
*E-mail addresses:* vokrouhl@cesnet.cz (D. Vokrouhlický), petr.pokorny@volny.cz (P. Pokorný), davidn@boulder.swri.edu (D. Nesvorný).

0019-1035/$ - see front matter © 2012 Elsevier Inc. All rights reserved.
doi:10.1016/j.icarus.2012.02.021

Author's personal copy



Keplerian elements: semimajor axis $a$, eccentricity $e$, inclination $i$, longitude of node $\Omega$, argument of pericenter $\omega$ and true anomaly $f$. The angles $i$, $\Omega$ and $\omega$ are defined with respect to a chosen inertial frame $(X,Y,Z)$.[1] The orbit intersects the $(X,Y)$ reference plane in ascending and descending nodes, where $f = f_0 \equiv -\omega$ and $f = f_0 \equiv \pi - \omega$, respectively. Denote $a'$ the heliocentric distance at either of the two intersections. Introduce a local reference basis $(\mathbf{e}_r, \mathbf{e}_\phi, \mathbf{e}_z)$ of three orthonormal vectors with the origin at the ascending or descending node, such that $\mathbf{e}_r$ is directed in the radial direction, $\mathbf{e}_\phi$ in the longitude direction and $\mathbf{e}_z$ along the $Z$ axis.[2]

The heliocentric position vector $\mathbf{r}$ describing the elliptic orbit of the particle reads

$$\mathbf{r}(f) = r(f)[\mathbf{a}\cos(\omega + f) + \mathbf{b}\sin(\omega + f)], \tag{1}$$

with $r(f) = a\eta^2/(1 + e\cos f)$, $\eta^2 = 1 - e^2$, and unit vectors $\mathbf{a}^{\mathrm{T}} = (\cos\Omega, -\sin\Omega, 0)$ and $\mathbf{b}^{\mathrm{T}} = (-\cos i\sin\Omega, \cos i\cos\Omega, \sin i)$. At the ascending node we have $\mathbf{a} = \mathbf{e}_r$ and $\mathbf{b} = \cos i\mathbf{e}_\phi + \sin i\mathbf{e}_z$, while at the descending node $\mathbf{a} = -\mathbf{e}_r$ and $\mathbf{b} = -\cos i\mathbf{e}_\phi + \sin i\mathbf{e}_z$. Expanding $\mathbf{r}(f)$ near the origin in the local $(\mathbf{e}_r, \mathbf{e}_\phi, \mathbf{e}_z)$ system (i.e., near the respective nodal intersection with the $(X,Y)$ reference plane), we obtain $\mathbf{r}(f) = a'\mathbf{e}_r + d\mathbf{r}$ with

$$d\mathbf{r} = a'\mathbf{A}_1\, df + \frac{a'}{2}\mathbf{A}_2\, df^2 + \mathcal{O}(df^3), \tag{2}$$

where $df$ is infinitesimal increment of the true anomaly with respect to the intersection value $f_0$. Eq. (2) locally describes particle's elliptic orbit, with $df$ being an affine parameter having values suitably close to zero. The first term is the crudest rectilinear approximation, while the second term describes the local curvature of the elliptic orbit. The first- and second-order vectorial coefficients read (upper sign for the ascending node intersection and lower sign for the descending node intersection)

$$\mathbf{A}_1 = \mp\frac{e\sin\omega}{P}\mathbf{e}_r + (\cos i\mathbf{e}_\phi \pm \sin i\mathbf{e}_z), \tag{3}$$

$$\mathbf{A}_2 = -2\left[1 - \frac{3}{2P} + \frac{\eta^2}{P^2}\right]\mathbf{e}_r - 2\frac{e\sin\omega}{P}(\pm\cos i\mathbf{e}_\phi + \sin i\mathbf{e}_z), \tag{4}$$

where $P = a\eta^2/a'$ and $\eta^2 = 1 - e^2$.

Consider now an observer moving on a circular heliocentric orbit with radius $a'$ in the $(X,Y)$ reference plane. Eq. (2) may be also used to describe its orbit near the respective nodal intersection with the eccentric orbit, with $\mathbf{A}_1^{\mathrm{circ}} = \mathbf{e}_\phi$ (henceforth also the apex direction), $\mathbf{A}_2^{\mathrm{circ}} = -\mathbf{e}_r$ and $df = df_{\mathrm{circ}}$, a differential in the observer's longitude. Denote $V_{\mathrm{circ}}$ the orbital velocity of the observer (given by the third Kepler law) and $V$ the relative velocity of the particle with respect to the observer. It is convenient to introduce a scaled value $v$ of the relative velocity, namely $v = V/V_{\mathrm{circ}}$, and parametrize the complete relative vector $\boldsymbol{v}^{\mathrm{T}} = (v_r, v_\phi, v_z) = v(\cos b\sin\ell, \cos b\cos\ell, \sin b)$ $v_\phi, v_z) = v(\cos b\sin\ell, \cos b\cos\ell, \sin b)$ with a longitude $\ell$ and a latitude $b$ of the radiant seen by the observer (henceforth, $\ell$ is measured from the apex direction and increases toward local radial direction in our notation). We also note that our choice makes $\boldsymbol{v}$ point *toward* the radiant from which the observer sees the particle impact.

The velocity components $(v_r, v_\phi, v_z)$ may be easily obtained from the linear term in (2), namely by using

$$\boldsymbol{v} = \mathbf{e}_\phi - \frac{1}{V_{\mathrm{circ}}}\left(\frac{d\mathbf{r}}{dt}\right)_{f=f_0} = \mathbf{e}_\phi - \mathbf{A}_1\sqrt{P}. \tag{5}$$

We thus obtain

$$e\cos\omega = \pm(P - 1), \tag{6}$$

$$e\sin\omega = \pm\sqrt{P}v_r, \tag{7}$$

$$\sqrt{P}\cos i = 1 - v_\phi, \tag{8}$$

$$\sqrt{P}\sin i = \mp v_z, \tag{9}$$

where the upper sign holds for the ascending node intersection and the lower sign for the descending node intersection. Here the first formula (6) is simply the geometric condition of intersection at heliocentric distance $a'$ (as stated above), and the next three formulas (7)–(9) specify the radiant location and impact velocity (in units of $V_{\mathrm{circ}}$). Obviously, our $(v_r, v_\phi, v_z)$ are closely related, in fact identical, to the standard velocity components $(U_x, U_y, U_z)$ introduced in the Öpik theory (see, e.g., Öpik, 1951, 1976).

Finally, it will be useful to rewrite beforehand Eq. (6) using the non-singular variables $k = e\cos\omega$ and $h = e\sin\omega$ and parameter $\alpha = a'/a$. In the $(k,h)$ plane the nodal intersection condition (6) reads

$$\left(k \pm \frac{\alpha}{2}\right)^2 + h^2 = 1 - \alpha + \frac{\alpha^2}{4}, \tag{10}$$

which is simply an equation of a circle displaced by $\pm\alpha/2$ on the $k$-axis for the ascending, resp. descending, node and radius equal to $\sqrt{1 - \alpha + \alpha^2/4}$.

## 3. Öpik collision probability approach

In the Öpik approach, the collision probability of a particle with a target is composed of two independent parts: (i) probability $P_1$ that during the secular cycle of the particle orbital elements its heliocentric node is close to the target's circular orbit (such that their distance can be small enough), and (ii) probability $P_2$ that the target is close to the nodal intersection of the particle orbit. A product of these statistically independent partial probabilities provides the total probability of impact per revolution of the particle: $P = P_1P_2$. Dividing this value by the orbital period of the particle then yields total probability per unit of time (this is because we assume an equilibrium distribution of particles along the impacting orbit). Obviously, in this way the resulting collision probability is a long-term averaged value or, equivalently, a population averaged value for a large population of particles in steady-state.

Because we keep the assumption of the circular motion of the target and the rectilinear representation of the particle motion near the nodal configurations (first term in Eq. (2)), analysis of $P_2$ is the same as in Öpik (1951). In particular, assuming the target with radius $R$ on a circular heliocentric orbit with radius $a_{\mathrm{circ}}$, we have

$$P_2(a,e,i) = \frac{R}{4a_{\mathrm{circ}}}\sqrt{\frac{3 - T(a,e,i)}{2 - F(a,e,i)}}, \tag{11}$$

with

$$T(a,e,i) = \frac{a_{\mathrm{circ}}}{a} + 2\sqrt{\frac{a}{a_{\mathrm{circ}}}}\eta\cos i, \tag{12}$$

$$F(a,e,i) = \frac{a_{\mathrm{circ}}}{a} + \frac{a}{a_{\mathrm{circ}}}\eta^2\cos^2 i. \tag{13}$$

However, to compute $P_1$, Öpik's assumed constant values of $e$ and $i$ and uniform circulation of $\omega$. This is an acceptable approximation for low inclination and low eccentricity orbits, but it fails when either of or both these elements are large. Our goal is to extend determination of $P_1$ for orbits with arbitrary inclination and eccentricity values.

[1] We assume $i \neq 0$, otherwise a non-singular set of orbital elements would be needed. In order to keep a close similarity in notation to the works of Öpik (1951) and Wetherill (1967) we only consider the non-planar case.

[2] Note that the $\mathbf{e}_r$ and $\mathbf{e}_\phi$ vectors at the descending node are opposite to their values in the descending node, and vice versa, in our definition.

Author's personal copy



### 3.1. Lidov–Kozai driven secular evolution of the particle orbit

We adopt a secular model for particle dynamics, namely assuming its orbit is not resonant with any of the perturbing massive bodies in the Solar system. For simplicity assume planets move on circular and coplanar orbits. Within this model, the first-order perturbations of particle dynamics are obtained by independent averaging of the perturbing function from an arbitrary number of planets over their mean longitude in orbit and that of the particle (e.g., Morbidelli, 2002). Such an approximation immediately provides two integrals of motion, notably (i) the semimajor axis $a$ of the particle, and (ii) projection of the orbital angular momentum on the symmetry axis of the planetary system (i.e., normal to the Laplace plane). The latter may be most conveniently expressed using a constant $c = \eta \cos i$, which implies that any variation in eccentricity $e$ (or $\eta$) is correlated with the corresponding variation of the inclination $i$. In other words, inclination may be considered as a dependent parameter on the eccentricity. The axial symmetry of the secular (averaged) problem also implies that the longitude of node $\Omega$ of the particle orbit is a dummy parameter in the perturbing function $\mathcal{P}$, which – apart from constants – depends only on two orbital parameters: eccentricity $e$ and argument of pericenter $\omega$ (or their canonical analogs within a Hamiltonian theory; see, e.g., Morbidelli, 2002). Finally, since averaging over planets' motion about the Sun eliminates time dependence of the perturbing function, its value itself is also an integral of motion: $\mathcal{P}(e,\omega; a,c) =$ constant. This again shows, that any secular variation in $\omega$ is reflected in a correlated way in the respective variations of $e$.

In the most general situation of multiple planets with particle orbit crossing all or some of them, the averaged perturbing function $\mathcal{P}(e,\omega; a,c)$ may be obtained only using numerical quadrature (e.g., Bailey et al., 1992; Thomas and Morbidelli, 1996; Gronchi and Milani, 1998, 1999; Morbidelli, 2002). It should be noted that the problem has, aside to numerical evaluation, also subtle conceptual (mathematical) difficulties related to averaging of perturbing function with singular points (cf., Gronchi and Milani, 1998). Our approach developed below might be applied to this case as well, but it would require to evaluate most of the necessary functions numerically. In order to better understand the situation we prefer to restrict to a simpler case, in which more computations could be developed analytically and thus more directly compared with the traditional Öpik's theory. In particular, we assume only one perturbing planet (Jupiter) and a particle orbit entirely inside its orbit. The Earth as a target is assumed massless, which is a fairly good approximation overall. In this case, $\mathcal{P}(e,\omega; a,c)$ may be obtained in terms of multipole series (e.g., Kozai, 1962), of which we shall retain only the leading quadrupole part. Unless perihelion of the particle orbit is close to Jupiter, this is again a fairly satisfactory assumption, at least for sake of our illustration.[3] Using these approximations, a number of constant terms may be factorized from expression of $\mathcal{P}(e,\omega; a,c)$, resulting then in an integral of motion in the form (e.g., Kozai, 1962; Kinoshita and Nakai, 2007)

$$\mathcal{H}(k,h;c) = \frac{1}{\eta^2}[(2+3e^2)(3c^2-\eta^2)+15(\eta^2-c^2)(k^2-h^2)] = C. \qquad (14)$$

Here, we introduce the non-singular variables $k$ and $h$ from Eq. (10). Topology of the $C$-conserved isolines in the $(k,h)$ plane for various values of $c$ and $C$ has been extensively studied (e.g., Kozai, 1962; Morbidelli, 2002) and we do not need to discuss it in detail. Suffice it to say that in the limit of $|c|$ large enough the level curves of constant $C$ are ovals about the origin of the $(k,h)$ plane that become near circular for $|c| \to 1$. In this limit, both eccentricity and inclination of the particle orbit are small and nearly conserved, matching thus the assumptions of the original Öpik collisional theory. We also note that for a given $c$ value, the eccentricity can take values up to a maximum $\sqrt{1-c^2}$ (more rigorous specification of the interval of $e$ and $i$ value for given $c$ and $C$ integrals can be found, for instance, in Kinoshita and Nakai, 2007, Eqs. (31) and (32). At the critical value $c^2 = 3/5$, topology of the level curves of the $C$ integral changes, adapting to bifurcation of two new stationary solutions at the $h$ axis (i.e., with $\cos\omega = 0$): (i) for $C > 2(3c^2-1)$ they still circulate about the origin, but may take excursions to a very large eccentricity value on the $h$ axis, and (ii) for $C < 2(3c^2-1)$ they circulate about the stationary points on the $h$ axis. Examples are later seen in Figs. 3 and 4.

### 3.2. Crossing configurations with a target of a finite size

The exact configurations of orbital intersection with a target on a circular heliocentric orbit with radius $a_{\rm circ}$ are determined as roots $k_\star$ and $h_\star$ of Eq. (10), or equivalently Eqs. (6) and (14) with $\alpha = a_{\rm circ}/a$. All of them can be computed analytically, leading to a problem of roots of a cubic equation for $k_\star$. Because of the inversion symmetry $h_\star \leftrightarrow -h_\star$, there is always an even number of roots with generic number of 4 or 8 (2 and 6 are singular cases).[4] As a result, there can be twice as many impact configurations for orbits with high inclination than in the low inclination regime (only 4). This has been known for a long time, in particular from studies of high-inclination meteoroid streams (e.g., Babadzhanov and Obrubov, 1992). Examples are shown in the left panels of Figs. 3 and 4.

Now, the $P_1$ probability in the Öpik approach stems from the fact that the target has a small but finite radius $R$ ($R \ll a_{\rm circ}$).[5] This means that also orbits with $k$ and $h$ values in a small neighborhood of $(k_\star, h_\star)$ could pass closer than distance $R$ from the center of the target and should be considered intersecting. The limiting configurations with $k_{\rm lim}$ and $h_{\rm lim}$ values are those for which the particle orbit is grazing at distance $R$ from the target's orbit.

In order to formulate such a condition, we use local description of the particle's elliptic orbits from Section 2, Eq. (2). Consider particle's orbit with nodal intersection of the $(X,Y)$ plane at a heliocentric distance $a'$ close to $a_{\rm circ}$.[6] Define the $(\mathbf{e}_r, \mathbf{e}_\phi, \mathbf{e}_z)$ reference frame with the origin at target's orbit at a longitude identical to particle's intersection point with the $(X,Y)$ plane – see Fig. 1 for illustration. Retaining just the linear representation in (2), the particle's position vector in our reference frame is given by

$$\Delta\mathbf{r}(\lambda) = a'\mathbf{A}_1\lambda + (a' - a_{\rm circ})\mathbf{e}_r + \mathcal{O}(\lambda^2), \qquad (15)$$

where we denoted $\lambda = df$; recall the values near $\lambda = 0$ describe the particle orbit near the nodal line. The vector $\mathbf{A}_1$ is given in Eq. (3) with $P = a\eta^2/a'$. In the same way, we may locally represent target's orbit in the same reference frame with

$$\Delta\mathbf{r}'(\lambda') = a_{\rm circ}\mathbf{e}_\phi\lambda' + \mathcal{O}(\lambda'^2), \qquad (16)$$

where we again retained just the linear term (the target's orbit is thus $\phi$ axis in our system). The square of the target-particle distance is simply $d^2(\lambda,\lambda') = [\Delta\mathbf{r}(\lambda) - \Delta\mathbf{r}'(\lambda')]\cdot[\Delta\mathbf{r}(\lambda) - \Delta\mathbf{r}'(\lambda')]$, and we seek a minimum orbital distance $d^2_{\rm min}$ as a minimization problem in the

[3] In any case, adding higher-multipole terms in the secular perturbing function is just a matter of more algebraic labor, but does not represent any conceptual obstacle to our approach.

[4] Apart from the mentioned symmetry, stemming from the fact that Eqs. (10) and (14) contain only $h^2$, there is also $k_\star \leftrightarrow -k_\star$ symmetry for impact configurations in the ascending and descending nodes of the particle orbit.

[5] In fact, the geometric radius $R$ of the target should be augmented by a factor $\sqrt{1+(V_{\rm esc}/V)^2}$, where $V_{\rm esc}$ is the escape velocity from the target and $V$ is the impact speed of the particle at a large distance from the target. This recalibration takes into account focusing effect of the target's gravitational field.

[6] Note, we need now to distinguish particle nodal distance $a'$ from the target's heliocentric distance $a_{\rm circ}$. This has to be kept in mind when consulting formulas from Section 2.

Author's personal copy



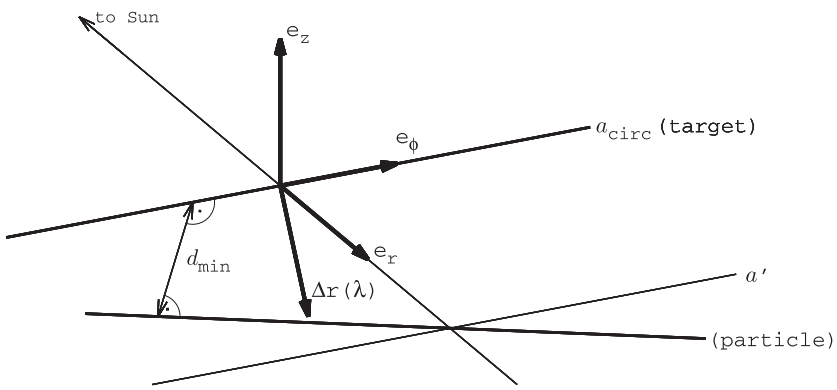


**Fig. 1.** Geometrical quantities used to represent particle and target motion near the intersection configuration. The reference frame $(\mathbf{e}_r, \mathbf{e}_\phi, \mathbf{e}_z)$ has the origin at the target's orbit: $\mathbf{e}_r$ in the radial direction from the Sun and $\mathbf{e}_\phi$ in the apex direction of the target's heliocentric motion (assumed circular with radius $a_{\rm circ}$). The particle's orbit has a node at heliocentric distance $a' \neq a_{\rm circ}$ and its position $\Delta\mathbf{r}$ in the local frame $(\mathbf{e}_r, \mathbf{e}_\phi, \mathbf{e}_z)$ is given by Eq. (15). We seek minimum distance $d_{\rm min}$ of the particle from target's orbit.

two-parametric $(\lambda, \lambda')$ space.[7,8] In the linear representations of $\Delta\mathbf{r}(\lambda)$ and $\Delta\mathbf{r}'(\lambda')$ the task is simple enough and yields

$$d_{\rm min} = (a' - a_{\rm circ}) \frac{P \sin i}{\sqrt{P^2 \sin^2 i + e^2 \sin^2 \omega}}, \tag{17}$$

with $a' = a\eta^2/(1 \pm e\cos\omega)$ for the ascending and descending node intersections. Scaling $d_{\rm min}$ by $a$ and making it equal to $\rho = R/a$, we obtain for the target-grazing orbits

$$\mathcal{K}(k, h; c) \equiv [\eta^2 - \alpha(1 \pm k)] \sqrt{\frac{\eta^2 - c^2}{(\eta^2 - c^2)(1 \pm k)^2 + h^2\eta^2}} = \rho. \tag{18}$$

Here, we used the secular representation of the orbital elements evolution, eliminating in particular inclination $i$ using $c = \eta\cos i$ integral. The $k_{\rm lim}$ and $h_{\rm lim}$ values are obtained by simultaneous solution of Eqs. (14) and (18). Unfortunately, this system of equations does not have simple analytical solutions. However, given that $\rho \ll 1$, we may seek small displacements $\delta k$ and $\delta h$ such that $k_{\rm lim} = k_\star + \delta k$ and $h_{\rm lim} = h_\star + \delta h$. Linearizing our problem in $\delta k$ and $\delta h$ we obtain

$$\delta k = -\rho \frac{(\partial\mathcal{H}/\partial h)_\star}{\mathcal{D}_\star}, \quad \delta h = \rho \frac{(\partial\mathcal{H}/\partial k)_\star}{\mathcal{D}_\star}, \tag{19}$$

where

$$\mathcal{D}_\star = (\partial\mathcal{K}/\partial h)_\star (\partial\mathcal{H}/\partial k)_\star - (\partial\mathcal{K}/\partial k)_\star (\partial\mathcal{H}/\partial h)_\star. \tag{20}$$

The symbol ★ here means that all derivatives have to be evaluated using the $(k_\star, h_\star)$ values corresponding to the exact intersection condition. After a brief algebra we find

$$(\partial\mathcal{H}/\partial k)_\star = \frac{2k_\star}{\eta_\star^2}\left[2\left(7 - 3c^2 - 12k_\star^2 + 3h_\star^2\right) + C\right], \tag{21}$$

$$(\partial\mathcal{H}/\partial h)_\star = \frac{2h_\star}{\eta_\star^2}\left[2\left(12c^2 - 8 + 3k_\star^2 + 18h_\star^2\right) + C\right], \tag{22}$$

$$(\partial\mathcal{K}/\partial k)_\star = -2\left(k_\star \pm \frac{\alpha}{2}\right)\sqrt{\frac{\eta_\star^2 - c^2}{(\eta_\star^2 - c^2)(1 \pm k_\star)^2 + h_\star^2\eta_\star^2}}, \tag{23}$$

$$(\partial\mathcal{K}/\partial h)_\star = -2h_\star\sqrt{\frac{\eta_\star^2 - c^2}{(\eta_\star^2 - c^2)(1 \pm k_\star)^2 + h_\star^2\eta_\star^2}}. \tag{24}$$

It turns out that the novel property of our approach are mainly the $(\partial\mathcal{H}/\partial k)_\star$ and $(\partial\mathcal{H}/\partial h)_\star$ derivatives, because the condition (18) and its partial derivatives remain formally the same as in the classical Öpik theory (see Appendix A, Eqs. (A7) and (A8)). Note that in the linear approximation, the $(\delta k, \delta h)$ solution is accompanied with a symmetric $(-\delta k, -\delta h)$ solution. Obviously, such displacements are along the tangent to the level line of the $\mathcal{H} = C$ integral at the $(k_\star, h_\star)$ point.

A second novel aspect of our approach, and a generalization of the classical Öpik theory, is that for each possible intersection configuration $(k_\star, h_\star)$ we determine time interval $(\Delta t)_\star$ it takes the particle orbit to evolve from $(k_\star - \delta k, h_\star - \delta h)$ to $(k_\star + \delta k, h_\star + \delta h)$, i.e. across the interval of values it may impact onto the target. The partial $P_1$ probability from this intersection configuration is then $(\Delta t)_\star/T_{\rm Kozai}$, where $T_{\rm Kozai}$ is the period of whole secular evolution along the level curve of the $C$ integral; $T_{\rm Kozai}$ may be evaluated using a complete elliptic integral of the first kind as shown by Kinoshita and Nakai (2007). We then define the Öpik-type collision probability of impact per revolution of the particle

$$P = \sum \left(\frac{\Delta t}{T_{\rm Kozai}}\right)_\star P_2(a, e_\star, i_\star), \tag{25}$$

which generalizes (A13) recalled in Appendix A. The summation in (25) is performed over all intersection configurations for both ascending and descending nodes. Note that, unlike in the Öpik approach, the orbital eccentricity $e_\star$ and inclination $i_\star$ is now different for different crossing configurations and we need to multiply the partial $P_1$ probability with the appropriate and individual $P_2$ probability that the target is near the intersection location. Because the semimajor axis value of the particle is constant, the intrinsic collision probability per unit of time is simply

$$p = P/T_{\rm orb} = (1/2\pi)(\sqrt{GM}/a^{3/2})P, \tag{26}$$

where $T_{\rm orb}$ is the orbital period of the particle and $M$ is the solar mass.

Finally, we return to the issue how to determine $(\Delta t)_\star$. The flow along the $C$ integral isoline is given by the differential equations (e.g., Kozai, 1962; Morbidelli, 2002; Kinoshita and Nakai, 2007)

[7] In our linear approximation things are simpler, and one may drop $\lambda'$ by just evaluating $\Delta\mathbf{r}(\lambda)$ distance from the $\phi$ axis. However, the two-parametric formulation might be important to keep in mind when higher-order approximations for $\Delta\mathbf{r}(\lambda)$ and/or $\Delta\mathbf{r}'(\lambda')$ would be used.

[8] Note that $d^2(\lambda, \lambda')$ is quadratic in $\lambda$. Its description using the linear approximation (15) might look incomplete, because the corresponding quadratic term (see, e.g., Eq. (2)) would also contribute to the quadratic term in $d^2$. However, a closer analysis reveals that this addition does not change our results. A more general Öpik collision theory, for instance suitable to describe impacts very close to the pericenter or apocenter of the particle orbit (see Appendix A), would require a complete analysis with $\mathbf{r}(\lambda)$ and $\mathbf{r}'(\lambda')$ represented by higher-order terms beyond the linear approximation used here (and in most previous works).

Author's personal copy



$$\frac{dk}{dt} = -\frac{3}{2}\gamma\eta h\left[1+\frac{5}{2}\frac{c^2(1-k^2)-\eta^4}{\eta^4}\right], \tag{27}$$

$$\frac{dh}{dt} = \frac{3}{2}\gamma\eta k\left[1+\frac{5}{2}\frac{c^2h^2}{\eta^4}\right], \tag{28}$$

where $\gamma = n\,(m/M)\,(a/a_{\rm Jup})^{3/2}$ with $n$ mean motion of the particle, $m$ mass of the Jupiter and $a_{\rm Jup}$ semimajor axis of its orbit; note we assume that the single perturber of the particle orbit is Jupiter. Given the linear solution of $\delta k$ and $\delta h$ above with typical values of the order $\rho(\ll 1)$, we found satisfactory to use a linear discretization of the differential Eqs. (27) and (28), namely representing $dk \to \delta k$, $dh \to \delta h$, $dt \to (\Delta t)_\star/2$ evaluating their right hand sides at $(k_\star, h_\star)$ values. Either of Eqs. (27) and (28) provide the same results, up to terms of the second order in $\rho$.

This approach only fails when the displacements $\delta k$ and $\delta h$ are large, a singular situation when $\mathcal{D}_\star$ is very near 0; this always occurs when $h_\star = 0$, but there might be also other cases in general. In the Öpik formalism limit this singularity happens when the particle's perihelion or aphelion are equal to radius $a_{\rm circ}$ of the target's orbit (see also Appendix A). For that reason, we abandon the simple approach above in this case and we solve Eqs. (14) and (18) numerically when $\mathcal{D}_\star \leqslant 0.05$ in Eq. (20). This provides an accurate determination of all possible intersection configurations. We then determine the corresponding $(\Delta t)_\star$ value using a numerical integration of the secular system (27) and (28) in between the grazing configurations.

### 3.3. Comparison with the standard Öpik's theory

Here we test the generalized collision probability theory and compare the results with those of the standard Öpik theory (see Appendix A for a comparison of the analytical aspects of the two methods). In our first test case, we calculate the Earth-impact rates for a population of particles that is perturbed by Jupiter (circular orbit, $a_{\rm Jup} = 5.2$ AU). The Earth is assumed to have a circular orbit with $a_{\rm circ} = 1$ AU).

This is a simplified system. In reality there are more perturbing planets, including the Earth itself, whose orbits are also evolving due to their mutual interactions. This latter effect is especially important, because it produces secular resonances in the planet-crossing region (e.g., Michel and Thomas, 1996; Michel and Froeschlé, 1997) and variations of $c$ and $C$. We will consider this more complicated case later in this section.

We conducted numerical tests to compare the collision probability $p$ from (26), which should be accurate for the high-inclination and/or high-eccentricity orbits, with the predictions of the Öpik theory, which should be only approximate in these cases.

As the secular evolution follows the $\mathcal{H}(k,h;c) = C$ isoline in the $(k,h)$ plane there are typically four or eight intersections with the target orbit. In order to compare $p$ with the collision probability obtained by the Öpik's method, we determine $p_{\rm Opik}(a,e,i)$ from Eq. (A14) at each point of the line defined by $\mathcal{H}(k,h;c) = C$,[9] and compute an average value $p_{\rm eff}$ as

$$p_{\rm eff} = \frac{1}{T_{\rm Kozai}}\int_0^{T_{\rm Kozai}} dt\, p_{\rm Opik}(a,e,i). \tag{29}$$

Here, $T_{\rm Kozai}$ is the period of the Lidov–Kozai cycle. Note that evaluation of (29) needs some care when either pericenter $q$ or apocenter $Q$ of the particle orbit becomes equal to the radius $a_{\rm circ}$ of the target's orbit. This is because

$$p_{\rm Opik} \propto \frac{1}{\sqrt{(a_{\rm circ}-q)(Q-a_{\rm circ})}}, \tag{30}$$

and in both cases Öpik's collision probability has a singularity (see, however, discussion in Appendix A). Nevertheless, as seen from (30), this singularity is integrable and classical numerical tools can be used to accurately evaluate $p_{\rm eff}$ (see, e.g., Press et al., 2007).

#### 3.3.1. Testing the theory: a simple setup

We first test things in the low-$e$ and low-$i$ limit, where the standard Öpik works well. The initial orbital elements of particles were set to be $a = 1.01$ AU, $e = 0.02$, $i = 3°$ and $\omega = 0°$. In this case, the Kozai constant $c \simeq 0.9984$ is very close to unity. We thus expect the eccentricity and inclination should be approximately conserved and the secular angles $\omega$ and $\Omega$ should uniformly precess. Indeed, Fig. 2 shows that the $\mathcal{H}(k,h;c) = C$ isoline in the $(k,h)$ plane deviates negligibly from a small circle about the origin. As expected, $p \simeq p_{\rm eff}$ in this case. The 0.1%-difference between $p$ and $p_{\rm eff}$ is of the order of variations of $p_{\rm Opik}$ within one secular cycle of the orbital evolution. This difference is partially due to slight variations in $e$ and nonlinearity of time dependence of $\omega$, but may also express a small internal inaccuracy by which we can evaluate both $p$ and $p_{\rm eff}$.

We now move to testing the methods in the Lidov–Kozai regime. We set $a = 1.4$ AU, $e = 0.2$, $i = 65°$, corresponding to $c \simeq 0.414 < \sqrt{0.6}$. Figs. 3 and 4 show the results for $\omega = 0°$ and $\omega = 60°$, respectively. The left panels show nature of the particle orbital evolution using the $\mathcal{H}(k,h;c) = C$ isoline in the $(k,h)$ plane and the two circles characterize nodal impact configurations with the Earth orbit (with $a_{\rm circ} = 1$ AU; see Eq. (10)); symbols at intersections of the respective curves highlight the exact impact geometries that could occur for this orbit during its secular evolution. There are eight of them in Fig. 3 and four of them in Fig. 4. The right panels show formally computed Öpik collision probability values $p_{\rm Opik}$ as a function of time during a timespan of one secular cycle $T_{\rm Kozai}$ of the particle evolution. The discontinuities, when $p_{\rm Opik}$ formally diverge, correspond to configurations of pericentric impact to the target.[10] The solid gray lines are $p$ and $p_{\rm eff}$ values; note, that in both cases $p_{\rm eff}$ is about twice larger than $p$, indicating that using the standard Öpik theory one would overestimate the collision probability value for these orbits. The middle panels show radiant positions of the impacting particles: the symbols are real radiants corresponding to the true intersection geometries indicated on the left panels, while the gray line are collections of "fake radiants". The latter were obtained by applying assumptions of the Öpik theory, namely constant values of eccentricity and inclinations to the orbit of particle at different phase of its Lidov–Kozai-driven evolution. Obviously such an approach is incorrect, but it has been used in some previous works (e.g., Nesvorný et al., 2011). Note that the angular distance $\delta$ of the fake radiants from apex direction is given by $\cos\delta = (\boldsymbol{v}\cdot\mathbf{e}_\phi)/v = (1-\sqrt{P}\cos i)/\sqrt{3-T(a,e,i)}$, see Eqs. (7)–(9). As a result, $\delta$ depends only on the semimajor axis $a$ and the Kozai constant $c$ of the particle orbit, both conserved during the particle secular evolution, and thus the fake radiants project on arcs of constant angular distance from the apex direction.[11] When a particle or-

[9] Obviously, application of the Öpik approach is not well justified for orbits with low $c$ value associated with significant $e$ and $i$ evolution; nevertheless, it has been used even in these cases in previous works (e.g., Galligan and Baggaley, 2005; Campbell-Brown, 2008; Nesvorný et al., 2011) and part of our work is to see a misfit represented by this inconsistency.

[10] Note, for instance, that the initial values of the orbital elements have a pericenter $q > a_{\rm circ}$ and no impact configuration is possible; it only takes a while during the secular evolution of the particle orbit before the eccentricity increases enough to make $q = a_{\rm circ}$.

[11] This fact has actually been known and used in the meteoritics; see, e.g., Valsecchi et al. (1999), where the secularly invariant value of $\delta$ ($\theta$ in the notation of this paper) plays a crucial role in defining the similarity function for meteoroid streams.

Author's personal copy



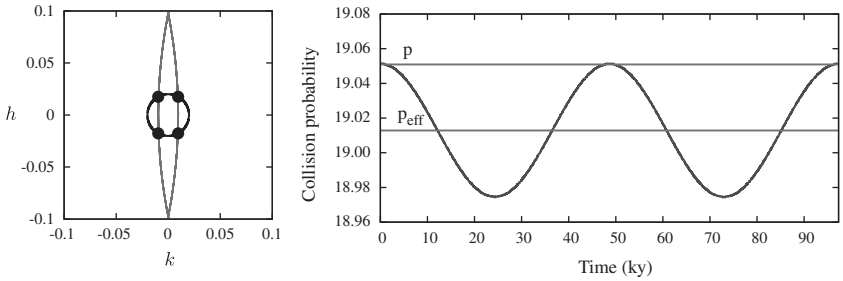


**Fig. 2.** Secular evolution and intrinsic impact probability for a particle orbit with initial semimajor axis $a = 1.01$ AU, eccentricity $e = 0.02$, inclination $i = 3°$ and argument of pericenter $\omega = 0°$. Left: $\mathcal{H} = C$ isoline in the $(k,h)$ plane of variables (black solid curve) and nodal intersection conditions with $a_{\rm circ} = 1$ AU for ascending and descending nodes (segments of gray circles; see Eq. (10)). Symbols are the four possible impact geometries. Right: Collision probability value $p_{\rm Opik}(a,e,i)$ formally computed using the Öpik formalism for time-dependent values of $e$ and $i$ as given by the secular evolution of the orbit; the abscissa is time in ky during one secular cycle $T_{\rm Kozai}$, and the ordinate is the intrinsic collision probability per AU$^2$ and yr. The horizontal lines are: (i) $p_{\rm eff}$ defined in Eq. (29), and (ii) the true collision probability $p$ defined in Eq. (25).

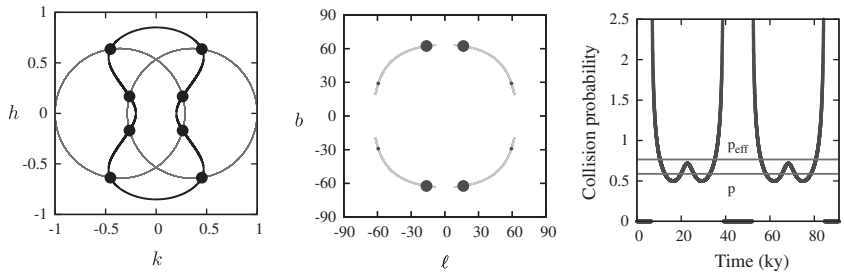


**Fig. 3.** Secular evolution and impact geometries for a particle orbit with initial semimajor axis $a = 1.4$ AU, eccentricity $e = 0.2$, inclination $i = 65°$ and argument of pericenter $\omega = 0°$. Left: $\mathcal{H} = C$ isoline in the $(k,h)$ plane of variables (solid curve) and nodal intersection conditions with $a_{\rm circ} = 1$ AU for ascending and descending nodes (gray circles; see Eq. (10)). Symbols are the eight possible impact geometries. Middle: Radiant position of the eight impacting configurations as seen by the observer on a circular heliocentric orbit with radius $a_{\rm circ} = 1$ AU; size of the symbol is scaled by the partial collision probability for this particular impact geometry. The gray arcs are collections of "fake radiants" constructed for orbits with constant eccentricities and inclinations, whose values are achieved during the secular evolution of the particle orbit. The abscissa is longitude measured from the apex direction, the ordinate is latitude (both in degrees). Right: Collision probability value $p_{\rm Opik}(a,e,i)$ formally computed using the Öpik formalism for time-dependent values of $e$ and $i$ as given by the secular evolution of the orbit; the abscissa is time in ky during one secular cycle $T_{\rm Kozai}$, and the ordinate is the intrinsic collision probability per AU$^2$ and yr. The horizontal lines are: (i) $p_{\rm eff}$ defined in Eq. (29), and (ii) the true collision probability $p$ defined in Eq. (25).

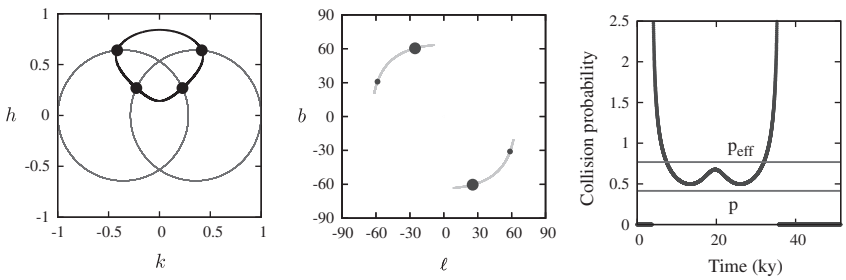


**Fig. 4.** The same as in Fig. 3 but for an orbit with initial semimajor axis $a = 1.4$ AU, eccentricity $e = 0.2$, inclination $i = 65°$ and argument of pericenter $\omega = 60°$.

bit circulates about a stable point on the $h$ axis, such as seen on Fig. 4, the argument of pericenter is forced to oscillate about 90° or 270° values, and the radiants asymmetrically populate only one quadrant in the longitude vs. latitude plane. The size of symbols denoting the correct radiants is scaled by the partial collision probability – $(\Delta t/T_{\rm Kozai})_\star P_2(a,e_\star,i_\star)$, see Eq. (25) – for this particular impact configuration. Note that the higher-latitude radiants have systematically larger collision probability (e.g., in Fig. 3 three times) than the lower-latitude radiants. This is because the particle orbit spends more time at the large-inclination, and low-eccentricity, state and thus $(\Delta t)_\star$ is larger for the high-inclination radiants.

In the two cases discussed above $p_{\rm eff} > p$, indicating that the true collision probability was smaller than the value given by the Öpik theory. We now consider the same parameters as those used in Fig. 3, but let the semimajor axis $a$ change to see how $p_{\rm eff}/p$ varies in general (Fig. 5). We find that $p_{\rm eff}/p > 1$, except if the impacts occur near the pericenter or apocenter, where $p_{\rm eff}/p < 1$.

Note the unusual extension of the impact probability line in Fig. 5 just below $Q = a_{\rm circ}$. Such a configuration is always an end-state of a sequence of impact possibilities in the Öpik approach, when eccentricity of the particle orbits is assumed constant. Fig. 6 helps to understand the situation. Shrinking the particle orbit semimajor axis makes $\alpha = a_{\rm circ}/a$ increase and the Earth-impact circles from Eq. (10) move toward larger $k$ values and shrink their radius in the $(k,h)$ plane. This would have lead to a "nominal" sequence of impact geometries 3′ to 1′ with no possibility of impact for the smallest $a$ value considered in this figure; in the same time the impact geometry 1′ would be exactly the end-member case with $Q = a_{\rm circ}$. When the secular evolution of the particle orbit is described by the more involved solid line $\mathcal{H}(k,h;c) = C$, impact

Author's personal copy



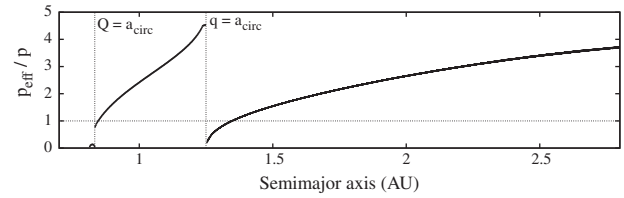


**Fig. 5.** The ratio $p_{\rm eff}/p$ shown as a function of the semimajor axis $a$ for orbits with fixed initial eccentricity $e = 0.2$, inclination $i = 65°$ and argument of pericenter $\omega = 0°$. The target's heliocentric distance is $a_{\rm circ} = 1$ AU. The discontinuities occur for initial orbits with pericenter $q$ or apocenter $Q$ equal to $a_{\rm circ}$. Only for orbits close to these geometries $p$ becomes larger than $p_{\rm eff}$, otherwise the use of Öpik formulation overestimates the collision probability with the target. The unusual feature below the formal $Q = a_{\rm circ}$ limit is explained using Fig. 6 (see discussion in the text).

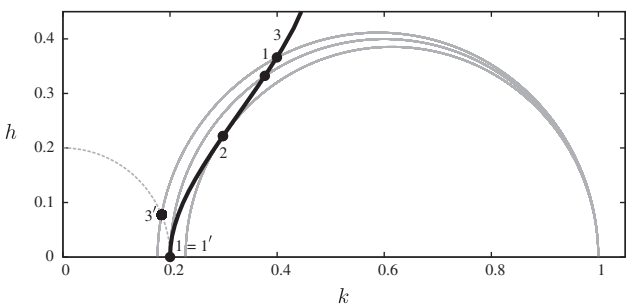


**Fig. 6.** Conditions for impacts near the apocenter of the particle orbit in the $(k,h) = e(\cos\omega, \sin\omega)$ plane of variables. The gray curves are the descending node impact circles from Eq. (10) for three slightly different values of $\alpha = a_{\rm circ}/a$ (smaller circle for a larger $\alpha$, thus smaller $a$, value). The solid black curve is a part of the $\mathcal{H}(k,h;c) = C$ isoline for certain values of $c$ and $C$ integrals of motion, describing secular evolution of a potentially impacting particle. The black symbols are impact geometries for various values of eccentricity of the particle. The impact case labeled $1 = 1'$ with $h = 0$, corresponding to apocenter condition $Q = a_{\rm circ}$, would have been in the Öpik theory an end-member of the possible family of impacts ($3' \to 1'$) along the family of constant eccentricity orbits shown by the dashed circle. For the true orbit an continuation of the impacts is possible up to the limiting case of grazing impact 2.

geometries are possible even after the apocenter geometry 1 has been reached. For smaller $a$ values the impact eccentricity may again increase up to the true end-member of the impact sequence at 2.

### 3.3.2. Testing the theory: a more realistic setup

We now compare the theory with the statistics of terrestrial impacts as recorded by a numerical integrator. We consider two sets of 500 massless particles having initially $a = 1.4$ AU, $e = 0.2$ and $i = 65°$. The argument of pericenter $\omega = 0°$ in the first set and $\omega = 60°$ in the second set. Nodal and orbit longitudes were taken randomly between 0° and 360°.

We first considered an idealized planetary system consisting of the Sun, Earth and Jupiter (both planets on circular orbits as before). The Earth was given zero mass and its radius was multiplied by a factor of 10 to accelerate the impact rate in the numerical integration ($R_{\rm Earth} = 4.26 \times 10^{-4}$ AU).

We numerically propagated the orbits of all bodies with the SWIFT_RMVS3 integrator,[12] using a 2-day time step, and recorded the direct impacts of particles on the Earth. Fig. 7 shows the fraction of particles surviving in our simulation as a function of time. For comparison, we also show the expected decay of the population assuming it can be modelled using a Poissonian processes with certain characteristic timescale $\tau$, thus $n_{\rm Pois}(t) = \exp(-t/\tau)$. The decay-curve labeled 1 has $\tau = \tau_1 \simeq 9.4$ Myr (upper panel) and

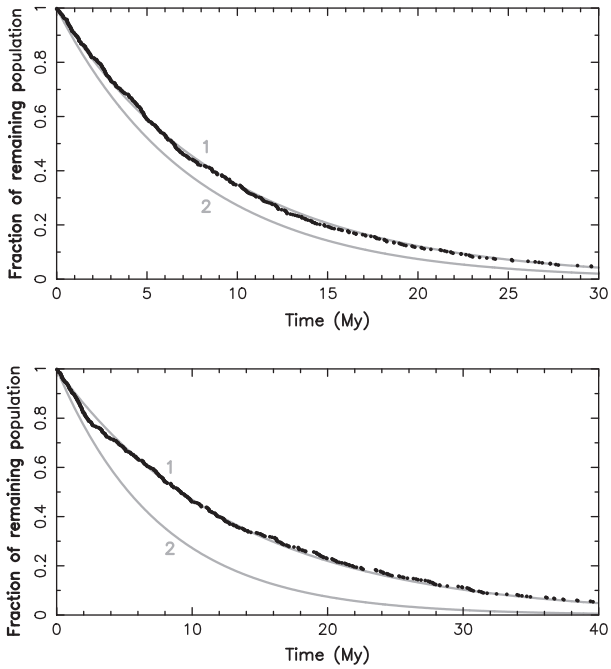


**Fig. 7.** Fraction of particle population remaining the numerical simulation shown by symbols vs. time $t$ (in Myr). 500 particles were initially put on orbits with semimajor axis $a = 1.4$ AU, eccentricity $e = 0.2$, inclination $i = 65°$ and argument of pericenter $\omega = 0°$ (upper panel) and $\omega = 60°$ (bottom panel); longitude of node and longitude in orbit were set randomly. Their orbital evolution was numerically propagated and direct impacts onto the Earth recorded in a reduced model where only Jupiter was considered on a circular heliocentric orbit (the Earth had zero mass a radius $R$ 10 times larger that the true value). The gray curves simulate results from a Poissonian process with a characteristic timescale $\tau$, thus $\exp(-t/\tau)$: (i) the curve 1 has $\tau \simeq 9.4$ Myr (upper panel) and $\tau \simeq 13.3$ Myr (bottom panel), corresponding to $1/(pR^2)$, and (ii) the curve 2 has $\tau \simeq 7.7$ Myr (both panels), corresponding to $1/(p_{\rm eff}R^2)$.

$\tau = \tau_1 \simeq 13.3$ Myr (bottom panel), while the decay-curves labeled 2 have $\tau = \tau_2 \simeq 7.7$ Myr (both upper and bottom panels).

We find that numerically recorded impact rate on the Earth very nicely matches the decay curves with $\tau = \tau_1$. This is because $\tau_1 = 1/(p\ R^2)$, where $p \simeq 0.586\ {\rm AU}^{-2}\,{\rm y}^{-1}$ (upper panel) and $p \simeq 0.413\ {\rm AU}^{-2}\,{\rm y}^{-1}$ (bottom panel) were determined using our generalized collisional probability theory (see Figs. 3 and 4). The probability $p$ therefore gives a simple and very good approximation for the real collisional decay. For comparison, the Öpik collision probability is $p_{\rm eff} \simeq 0.715\ {\rm AU}^{-2}\,{\rm y}^{-1}$ (upper panel) and $p_{\rm eff} \simeq 0.716\ {\rm AU}^{-2}\,{\rm y}^{-1}$ (bottom panel), and $\tau_2 = 1/(p_{\rm eff}\ R^2)$ decay in Fig. 7. Henceforth, we verified that the standard Opik theory would suggest a stronger decay than the actual one.

We also determined the direction of impacts in the numerical integrations described above. We found that the simulated particles indeed hit the Earth from the two discrete radiant locations shown in Figs. 3 and 4. The impacts from the higher-latitude radiants are approximately three times more numerous than those from the lower-latitude radiants. This is in a very good agreement with expected number of impacts in these radiants from our new theory.

We now consider a more realistic model of the Solar System where we take into account the gravitational perturbations between all planets. To prevent particles from impacting the terrestrial planets other than Earth, we set the physical radii of Mercury, Venus and Mars to zero. The Earth's radius is increased by a factor of 10. We consider the same two particle populations as before. The system was numerically integrated with SWIFT_RMVS3.

[12] http://www.boulder.swri.edu/~hal/swift.html.

Author's personal copy



Now, Jupiter is not the sole perturber of particle orbits, and the planetary orbits undergo secular variations due to mutual perturbations. In addition, close approaches of particles to the terrestrial produce a random walk in their orbits and affect the secular evolution. The evolving system is therefore more complex than the simple Lidov–Kozai model that we used in our generalized theory.

Fig. 8 shows how the fraction of the initial population remaining in the simulation decreases with time for the two simulations. Focusing first on the former case, we note that the particle population decay follows on average the expected Poissonian curve 1 (corresponding to the characteristic collision timescale $\tau = 1/(p R^2) \simeq 9.4$ Myr). However, initially the particles are being eliminated slightly faster while only at later epochs the rate of their elimination becomes slightly slower than shown by the idealized curve 1. We believe this is partly because of the particle-orbit scattering by the terrestrial planets, such that some particles are scattered onto orbits with smaller semimajor axis value and have effectively larger collision probability with the Earth, while the remaining population of particles is biased toward somewhat larger semimajor axis values with smaller collision probability with the Earth.

The situation is somewhat different in the bottom panel of Fig. 8, where the particle orbits had initially $\omega = 60°$. This is the case, when the argument of pericenter $\omega$ would circulate about a stationary point on the $h$ axis, making $\omega$ oscillate in a limited range of values, in the idealized Lidov–Kozai model (see the left panel on Fig. 4). However, this particular behavior of the orbits is quickly removed by both semimajor axis change due to scattering on terrestrial planets and a complex set of secular perturbations. As a result, the particle orbits more often spend their secular evolution in the mode similar to that seen in Fig. 3, with $\omega$ circulating about origin in the $(k,h)$ plane. The collision probability with the Earth then effectively increases and the decay rate approaches that from the above panel (shown by the dashed gray curve).

Finally, we propagated the first set of particles (initial value $\omega = 0°$) in the case where all terrestrial planets were taken as potential targets. To speed up the comparison, we increased the planetary radii by a factor of 10.

We used our collision probability theory to calculate $p_i$ for each planet ($i = 1 \cdots 4$, where 1 stands for Mercury, etc.), Denoting $R_i$ the enhanced radii of the terrestrial planets, the total collisional probability per year is $\Pi_{\rm tot} = \sum_i p_i R_i^2$. The particle population is thus expected to decay with a characteristic timescale $\tau \simeq 1/\Pi_{\rm tot} \simeq 3.9$ Myr. At each instant, the number of impacts on each of the terrestrial planets is weighted using their partial impact probabilities, i.e., $\propto p_i R_i^2/\Pi_{\rm tot}$ for the $i$th planet. These predictions are confronted with results from the numerical experiment in Fig. 9, where the symbols show the recorded planetary impacts for each of the planet and the dashed gray exponential decay curves are the above described theoretical predictions. While generally showing a good match, the solid gray decay curves slightly better express the population decrease and those have $\tau \simeq 3.2$ Myr.

The small difference between the theory and numerical experiment probably stems from the approximations in our collisional probability approach, where complex planetary perturbations and close encounters of particles to planets are neglected. Obviously, the whole particle population now decays faster than seen in Fig. 8 because more targets are available to destroy them. As expected all planet impacts are fitted by roughly the same decay rate, basically that of the whole population, and their partitioning is roughly that expected from the theory.

Mercury received a large number of impacts, more than it could be expected just based on its relatively small cross-section. This is because the partial impact probability, $p_1 R_1^2$, is increased by a large value of $p_1$ (nearly three times larger than that of the Earth). This can be explained by realizing that the Mercury impacts always occur near the pericenter of the particle orbits. Such impacts are characterized by large impact probability.

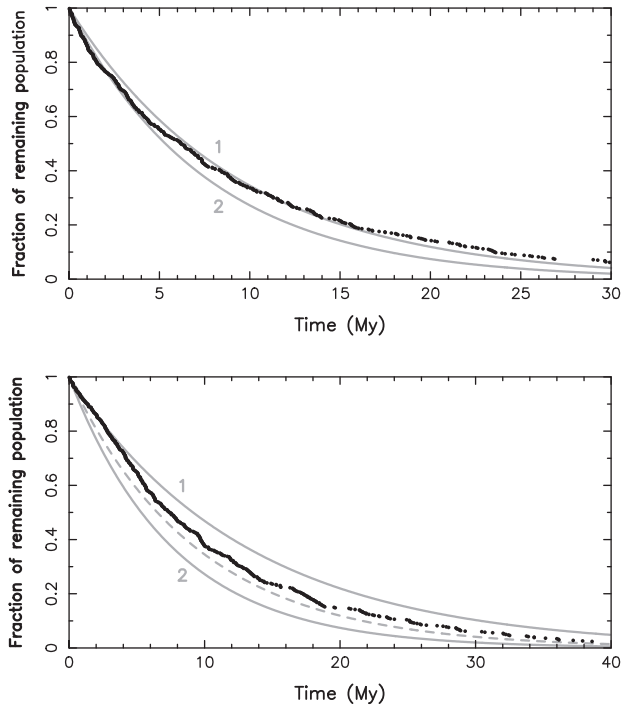


**Fig. 8.** Fraction of particle population remaining the numerical simulation shown by symbols vs. time $t$ (in Myr). 500 particles were initially put on orbits with semimajor axis $a = 1.4$ AU, eccentricity $e = 0.2$, inclination $i = 65°$ and argument of pericenter $\omega = 0°$ (upper panel) and $\omega = 60°$ (bottom panel); longitude of node and longitude in orbit were set randomly. Their orbital evolution was numerically propagated and direct impacts onto the Earth recorded in a model where perturbations from all planets were taken into account; impacts on Mercury, Venus and Mars were prevented by taking their radii zero and the Earth radius $R$ was 10 times larger that the true value. The gray curves simulate results from a Poissonian process with a characteristic timescale $\tau$, thus $\exp(-t/\tau)$: (i) the curve 1 has $\tau \simeq 9.4$ Myr (upper panel) and $\tau \simeq 13.3$ Myr (bottom panel), corresponding to $1/(pR^2)$, and (ii) the curve 2 has $\tau \simeq 7.7$ Myr (both panels), corresponding to $1/(p_{\rm eff} R^2)$. The dashed gray line in the bottom panel reproduces the solid line 1 from the top panel.

## 4. Conclusions

We developed a new collision probability theory for the high inclination and high eccentricity orbits for which the Lidov–Kozai cycles are important. The results of this theory agree with those of the standard Öpik theory in the limit of small-eccentricity and small-inclination orbits. For high eccentricities and high inclinations, where the standard Öpik theory falls short in correctly predicting the rates and radiants of the impacts, the generalized theory produces satisfactory results when compared to numerical experiments.

The theory developed in this paper can be generalized further, for example, by relaxing the assumption of the circular orbit of the target (Wetherill, 1967; Greenberg, 1982). Such a formulation may be required, for example, to properly calculate the planetary impact rates of during the early evolution of the Solar system (see, e.g., Bottke et al., 2005).

Another possibility would be to relax the linear approximation (15) and (16) for the local description of motion in the nodal reference system ($\mathbf{e}_r, \mathbf{e}_\phi, \mathbf{e}_z$), for instance by using the quadratic or higher-order approximations. This may be of some interest for improving the collision probability estimate in cases when the

Author's personal copy



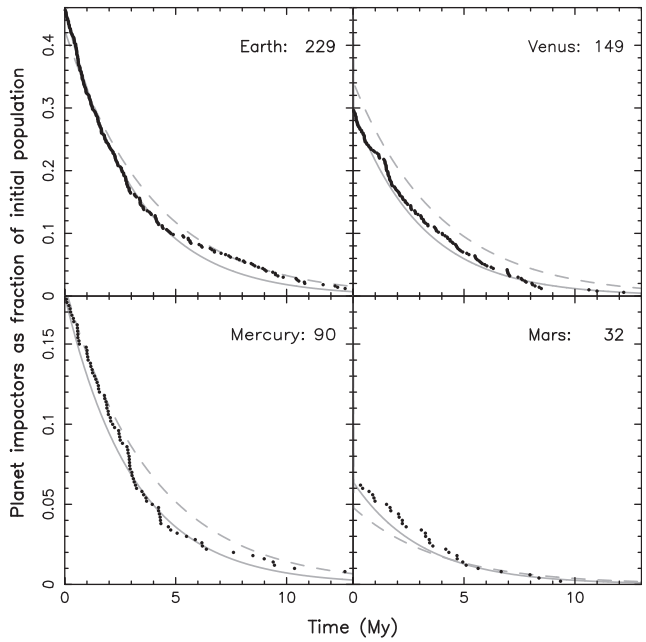


**Fig. 9.** Fraction of particles impacting the terrestrial planets in the most complete simulation, where all planets were considered as potential targets (their radii were increased by a factor 10 to speed up the simulation). The total number of impacts is indicated by labels. The dashed gray decay curves were obtained by an appropriate partitioning of the total decay of the particle population from our model, and the solid gray decay curves were the best match of the data (see the text).

curvature of orbits becomes important (e.g., for impacts near pericenter or apocenter of the particle orbit).


## Acknowledgements

This research was supported by Czech Grant Agency (Grants 205/08/0064 and 205/08/H005) and the Research Program MSM0021620860 of the Czech Ministry of Education. The work of DN was supported by the NASA Planetary Geology and Geophysics program. We thank Giovanni B. Valsecchi and Giovanni F. Gronchi, whose referee comments helped to improve the original version of this paper.


## Appendix A. Öpik's approximation

In what follows, we show that the general approach from Section 3.2 reproduces Öpik's results for appropriate assumption about the secular evolution of the particle orbit. In particular, the uniform circulation of the orbit in the $(k,h)$ plane on a circle of constant eccentricity $e$ is generated with

$$\mathcal{H}_{\rm Opik}(k,h) = k^2 + h^2 = C \tag{A1}$$

that follows from (14) in the limit of small $e$ value. When inclination $i$ is also small, conservation of $c = \eta\cos i$ implies $i$ = constant, and nodal circulation decouples from pericenter evolution. The condition (18) of particle grazing the target at a distance equal to its radius $R$ is given by

$$\mathcal{K}_{\rm Opik}(k,h;i) = [\eta^2 - \alpha(1\pm k)]\frac{\sin i}{\sqrt{h^2 + (1\pm k)^2\sin^2 i}} = \rho, \tag{A2}$$

where we recall $\rho = R/a$ and $a$ is the semimajor axis of particle orbit (recall $\alpha = a_{\rm circ}/a$ with $a_{\rm circ}$ heliocentric distance of the target).

First, let us again seek roots of (A1) and (A2) as small displacements $\delta k$ and $\delta h$ from exact intersection solution $k_\star$ and $h_\star$ given by (upper sign for the ascending node, lower sign for the descending node impacts)

$$1 \pm k_\star = \frac{\eta^2}{\alpha}, \tag{A3}$$

and

$$h_\star^2 = \frac{\eta^2}{\alpha^2}(\alpha - 1 + e)(1 + e - \alpha). \tag{A4}$$

Obviously, these are just geometrical conditions of intersections of two circles in the $(k,h)$ plane, namely $e$ = constant and (10). The $\delta k$ and $\delta h$ are obtained from (19), where now

$$(\partial\mathcal{H}_{\rm Opik}/\partial k)_\star = 2k_\star, \tag{A5}$$

$$(\partial\mathcal{H}_{\rm Opik}/\partial h)_\star = 2h_\star, \tag{A6}$$

$$(\partial\mathcal{K}_{\rm Opik}/\partial k)_\star = -\frac{2(k_\star \pm \alpha/2)\sin i}{\sqrt{h_\star^2 + (1\pm k_\star)^2\sin^2 i}}, \tag{A7}$$

$$(\partial\mathcal{K}_{\rm Opik}/\partial h)_\star = -\frac{2h_\star \sin i}{\sqrt{h_\star^2 + (1\pm k_\star)^2\sin^2 i}}, \tag{A8}$$

and thus

$$\mathcal{D}_\star = \mp\frac{2\alpha h_\star \sin i}{\sqrt{h_\star^2 + (1\pm k_\star)^2\sin^2 i}}. \tag{A9}$$

One easily verifies, that $(\delta k, \delta h)$ are small displacements along tangent to the circle $C = e^2$= constant. This is because the associated change in $e$ is $\delta e = (k_\star\delta k + h_\star\delta h)/e = 0$. In the same way, the associated change in argument of pericenter $\omega$ is $\delta\omega = (k_\star\delta h - h_\star\delta k)/e^2$, or

$$\delta\omega = \frac{\rho}{\alpha\sin i}\sqrt{1 + \frac{(1\pm k_\star)^2}{h_\star^2}\sin^2 i}. \tag{A10}$$

Inserting $k_\star$ and $h_\star$ from (A3) and (A4) above, we have

$$\delta\omega = \frac{R}{a_{\rm circ}\sin i}\sqrt{\frac{2 - F(a,e,i)}{2 - F(a,e,0)}}, \tag{A11}$$

with $F$-function defined in Eq. (13). The total advancement $\Delta\omega$ of the argument of pericenter between the two extreme, target-grazing configurations is $\Delta\omega = 2\delta\omega$. Because there are four equivalent intersection configurations at the ascending and descending nodes, we have

$$P_{1,\rm Opik} = \frac{2\Delta\omega}{\pi} = \frac{4}{\pi}\frac{R}{a_{\rm circ}\sin i}\sqrt{\frac{2 - F(a,e,i)}{2 - F(a,e,0)}}. \tag{A12}$$

Combining with $P_2$ from Eq. (11), this finally provides collision probability per revolution

$$P_{\rm Opik} = P_{1,\rm Opik}P_2 = \frac{1}{\pi}\frac{R^2}{a_{\rm circ}^2\sin i}\sqrt{\frac{3 - T(a,e,i)}{2 - F(a,e,0)}}, \tag{A13}$$

which is identical to results given by Öpik (1951) and Wetherill (1967), when restricted to circular orbit of the target (field body). The intrinsic collision probability per unity of time is again

$$p_{\rm Opik} = P_{\rm Opik}/T_{\rm orb} = (1/2\pi)(\sqrt{GM}/a^{3/2})P_{\rm Opik}, \tag{A14}$$

where $T_{\rm orb}$ is the orbital period of the particle (compare with Eq. (26)).

While obtaining identical result as previous authors in the limit of assumptions matching the classical Öpik theory, we finally comment on one of its well-known and often repeated aspects. In particular, the denominator term in the square-root factor in Eq. (A11), and consequently also (A12) and (A13), reads

Author's personal copy



$$2 - F(a,e,0) = \frac{(a_{\rm circ} - q)(Q - a_{\rm circ})}{a a_{\rm circ}}, \tag{A15}$$

where we denoted $q = a(1-e)$ and $Q = a(1+e)$, i.e., pericenter and apocenter distance of the particle orbit. This produces a singularity of the Öpik collision probability when pericenter or apocenter distances of the particle orbit become equal to the target's heliocentric distance. It seems to have passed unnoticed so far that this apparent singularity may be removed within the Öpik approach by a more thorough analysis of the impact geometries near the pericenter or apocenter configurations. In particular, it stems only from the *linearization* of small displacements about the exact impact geometry at $(k_\star, h_\star)$. However, the system of Eqs. (A1) and (A2) is simple enough to admit exact analytic solution. In particular, the roots in $k$ satisfy a simple quadratic equation $Ak^2 + 2Bk + C = 0$, with coefficients (upper sign for the ascending node, lower sign for the descending node)

$$A = \alpha^2 \sin^2 i + \rho^2 \cos^2 i, \tag{A16}$$

$$B = \pm[\alpha(\alpha - \eta^2) - \rho^2] \sin^2 i, \tag{A17}$$

$$C = (\alpha - \eta^2)^2 \sin^2 i - \rho^2 (e^2 + \sin^2 i). \tag{A18}$$

There are obviously two solutions $k_1^\pm$ and $k_2^\pm$

$$k_1^\pm = \frac{\mp[\alpha(\alpha - \eta^2) - \rho^2] \sin^2 i + \rho\sqrt{D(a,e,i)}}{\alpha^2 \sin^2 i + \rho^2 \cos^2 i}, \tag{A19}$$

$$k_2^\pm = \frac{\mp[\alpha(\alpha - \eta^2) - \rho^2] \sin^2 i - \rho\sqrt{D(a,e,i)}}{\alpha^2 \sin^2 i + \rho^2 \cos^2 i}, \tag{A20}$$

with

$$D(a,e,i) = \alpha\eta^2 F(a,e,i) \sin^2 i + \rho^2 (1 - \eta^2 \cos^2 i), \tag{A21}$$

and $F(a,e,i)$ from Eq. (13). To each of $k_1^\pm$ and $k_2^\pm$ we have corresponding $h_1^\pm = \sqrt{e^2 - k_1^{\pm 2}}$ and $h_2^\pm = \sqrt{e^2 - k_2^{\pm 2}}$ on the positive side of the $h$-axis and symmetric values on the negative side of the $h$-axis. We then simply determine the range $\Delta\omega^\pm$ of the argument of pericenter value around ascending and descending node intersection that still admit impact on the target with

$$\cos \Delta\omega^\pm = \frac{k_1^\pm k_2^\pm + h_1^\pm h_2^\pm}{e^2}. \tag{A22}$$

These values may be then used to compute the partial probabilities $P_{1,\rm Opik} = (\Delta\omega^+ + \Delta\omega^-)/\pi$. Nevertheless, even in this approach a care must be paid to configurations when impacts occur near pericenter or apocenter of the particle orbit. This is because in these cases one of the values $k_1^+$ or $k_2^-$ may become larger than $e$, which would prevent to compute the associated $h$ value. The reason for this effect is that the intervals $\Delta\omega$ for the impact configurations with positive and negative $h$ value are no more discontinuous and join together.

An example is seen in Fig. 10, where we show

$$\left(\frac{d_{\rm min}}{R}\right)^2 = \frac{[\eta^2 - \alpha(1+k)]^2 \sin^2 i}{h^2 + (1+k)^2 \sin^2 i}, \tag{A23}$$

as a function of $h$ near values where $h \sim 0$ (i.e., pericentric impacts in the ascending node). For sake of definiteness we took $e = 0.2$, $i = 25°$, $a_{\rm circ} = 1$ AU and $R$ equal to the Earth radius and plotted the left hand side for three different $a$ values of the particle orbit such that the corresponding $q$ value gets very close to $a_{\rm circ}$. Recall that, for a given particle orbit, $d_{\rm min}$ gives a minimum orbit distance from the target as a function of $(k,h)$, such that $d_{\rm min} \leqslant R$ characterize impact configurations. In general, intervals of $h$ values, which are straightforwardly mapped onto intervals of $\omega$ values, for which $(d_{\rm min}/R) \leqslant 1$ are disconnected on the positive and negative sides of the axis (light gray curves). But as one approaches the exact pericentric configuration, both intervals join together (black curve). In that case, $P_{1,\rm Opik}$ must be computed only from the common interval of $\omega$ values that overlap both impact configurations. Obviously, this way there is no exact singularity even for the pericentric impact.

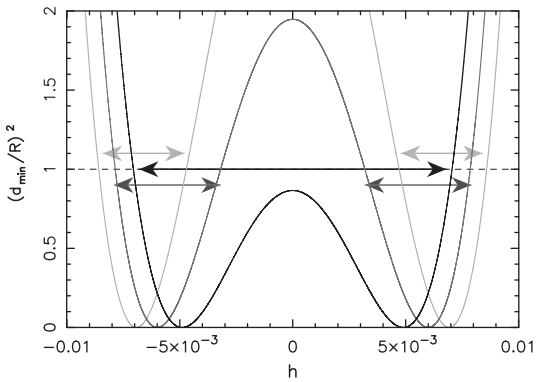


**Fig. 10.** Behavior of $(d_{\rm min}/R)^2$ function near exact intersection configurations at ascending node vs. $h$ (the $k$ value is constrained by a condition $k^2 + h^2 = e^2$ = constant). We show the situation for $h \sim 0$, i.e. when the impacts occur very near the pericenter of the particle orbit. Having the target orbit at $a_{\rm circ} = 1$ AU, we show three different cases: (i) $a_{\rm circ} - q = 10^{-4}$ AU (light gray), (ii) $a_{\rm circ} - q = 7.5 \times 10^{-5}$ AU (dark gray), and (iii) $a_{\rm circ} - q = 5 \times 10^{-5}$ AU (black), all for $R = 4.6 \times 10^{-5}$ AU equal to the Earth radius. The $(d_{\rm min}/R)^2 = 0$ condition is for the particle nodal distance exactly at $a_{\rm circ}$, denoted $h_\star$ in the text. The arrows indicate interval of $h$ values near $h_\star$ for which the minimum orbit distance to the target is less than $R$ and oblique impacts occur. There are usually separate $h$ (and correspondingly $\omega$) intervals for $h_\star$ positive and negative, but when $a_{\rm circ} - q$ is less than a critical value they merge into a single interval (such as for the black curve).

Note, however, that $\rho \sim 5 \times 10^{-5}$ in our example, and $\Delta\omega$ for near pericentric impacts is several orders of magnitude larger than $\rho$ (though not infinite). This means that the target-grazing configurations occur very far from the ascending node position of the exact particle impact at a heliocentric distance $a_{\rm circ}$. In this situation, the linear approximations for the particle and target orbits from Eqs. (15) and (16) are not justified and higher-order terms accounting for curvature of the local orbit would be necessary. As a result, our comment about nonexistent singularity in $P_{\rm Opik}$ is rather a curiosity than of real importance.

## References


Babadzhanov, P.B., Obrubov, Yu.V., 1992. Evolution of short-period meteoroid streams. Celest. Mech. Dynam. Astron. 54, 111–127.

Bailey, M.P., Chambers, J.E., Hahn, G., 1992. Astron. Astrophys. 257, 315–322.

Bottke, W.F., Durda, D.D., Nesvorný, D., Jedicke, R., Morbidelli, A., Vokrouhlický, D., Levison, H.F., 2005. Linking the collisional history of the main asteroid belt to its dynamical excitation and depletion. Icarus 179, 63–94.

Campbell-Brown, M.D., 2008. High resolution radiant distribution and orbits of sporadic radar meteoroids. Icarus 196, 144–163.

Galligan, D.P., Baggaley, W.J., 2005. The radiant distribution of AMOR radar meteors. Mon. Not. R. Astron. Soc. 359, 551–560.

Greenberg, R., 1982. Orbital interactions – A new geometrical formalism. Astron. J. 87, 184–195.

Gronchi, G.F., Milani, A., 1998. Averaging on Earth-crossing orbits. Celest. Mech. Dynam. Astron. 71, 109–136.

Gronchi, G.F., Milani, A., 1999. The stable Kozai state for asteroids and comets. With arbitrary semimajor axis and inclination. Astron. Astrophys. 341, 928–935.

Kessler, D.J., 1981. Derivation of the collision probability between orbiting objects. The lifetimes of Jupiter's outer moons. Icarus 48, 39–48.

Kessler, D.J., Cour-Palais, B.G., 1978. Collision frequency of artificial satellites: The creation of a debris belt. J. Geophys. Res. 83, 2637–2646.

Kinoshita, H., Nakai, K., 2007. General solution of the Kozai mechanism. Celest. Mech. Dynam. Astron. 98, 67–74.

Kozai, Y., 1962. Secular perturbations of asteroids with high inclination and eccentricity. Astron. J. 67, 591–598.

Lidov, M.L., 1961. Evolution of the planets artificial satellites orbits under effect of the outer bodies gravity perturbations. Artif. Satell. Earth 8, 5–45 (in Russian).

Lidov, M.L., 1962. The evolution of orbits of artificial satellites of planets under the action of gravitational perturbations of external bodies. Planet. Space Sci. 9, 719–759 (the English translation of Lidov's 1961 paper).

Michel, P., Froeschlé, Ch., 1997. The location of linear secular resonances for semimajor axes smaller than 2 AU. Icarus 128, 230–240.

Author's personal copy



Michel, P., Thomas, F., 1996. The Kozai resonance for near-Earth asteroids with semimajor axes smaller than 2 AU. Astron. Astrophys. 307, 310–318.
Morbidelli, A., 2002. Modern Celestial Mechanics: Aspects of Solar System Dynamics. Taylor & Francis, Cambridge Scientific Publishers, 376pp.
Nesvorný, D., Vokrouhlický, D., Pokorný, P., Janches, D., 2011. Dynamics of dust particles released from Oort cloud comets and their contribution to radar meteors. Astrophys. J. 743, 37, 12pp.
Öpik, E.J., 1951. Collision probabilities with the planets and the distribution of interplanetary matter. Proc. Roy. Irish A 54, 165–199.
Öpik, E.J., 1976. Interplanetary Encounters: Close-Range Gravitational Interactions. Elsevier, Amsterdam, 155pp.
Press, W.R., Teukolsky, S.A., Vetterling, W., Flannery, B.P., 2007. Numerical Recipes: The Art of Scientific Computing. Cambridge University Press, Cambridge, 1256pp.
Steel, D.I., Baggaley, W.J., 1985. Collisions in the Solar System – I: Impacts of the Apollo–Amor–Aten asteroids upon the terrestrial planets. Mon. Not. R. Astron. Soc. 212, 817–836.
Steel, D.I., Elford, W.G., 1986. Collisions in the Solar System: III – Meteoroid survival times. Mon. Not. Roy. Astron. Soc. 218, 185–199.
Sykes, M.V., 1990. Zodiacal dust bands: Their relation to asteroid families. Icarus 85, 267–289.
Thomas, F., Morbidelli, A., 1996. The Kozai resonance in the outer Solar System and the dynamics of long-period comets. Celest. Mech. Dynam. Astron. 64, 209–229.
Valsecchi, G.B., Jopek, T.J., Froeschlé, C., 1999. Meteoroid stream identification: A new approach I. Theory. Mon. Not. R. Astron. Soc. 304, 743–750.
Wetherill, G.W., 1967. Collisions in the asteroid belt. J. Geophys. Res. 72, 2429–2444.